Experimental Investigations and Modeling of the Rubber-Asphalt Sliding Pair Dynamics

Ante Božić[1,*] - Ivan Petrović[2] - Jadranko Matuško[2.]
[1] Volumtran, Compiegne, France
[2] University of Zagreb, Faculty of Electrical Engineering and Computing, Department of Control and
Computer Engineering, Zagreb, Croatia

A laboratory model for experimental investigations of the rubber-asphalt sliding pair has been designed to better understand the dynamic behavior of the friction force in the contact patch between the car tire and the road. Its design is described and some experimental results are given. These results confirm that in order to describe friction force in contact between the car tire and the road it is essential to use a dynamic friction model. Moreover, they indicate that the existing dynamic friction models might be physically incorrect in regards to the change of friction coefficient for an asperity bristle passing through the contact surface.
Keywords: car tires, Rubber-Asphalt sliding pair, road surfaces, sliding, friction force

0 INTRODUCTION

Adhesion quality of car tires significantly impacts the safety of car driving. During moderate speed driving on dry, clean and high quality roads, passive mechanic systems are able to provide satisfactory adhesion of the car tire to the road i.e. satisfactory dynamic behavior of the car. However, in high speed driving conditions and wet and low quality roads, dynamic behavior of the car during the acceleration, deceleration, and cornering may be far from the satisfactory one. With the purpose of improving the cars' controllability, they are often equipped with mechatronic systems for active vehicle dynamic control [1].

For understanding of vehicle controllability, as well as for the development and implementation of the specified solutions, it is important to understand the dynamics of friction force generated in contact between the car tire and the road. In that contact patch, complex dynamic processes occur as a consequence of combined action of rolling friction and sliding friction. Friction force is usually considered as a static force that is nonlinearly dependent on the sliding speed, while dynamic effects in contact patch are explained as a consequence of the deformation of the tire or some of its parts. Such an approach of describing the dynamic processes in contact between the tire and the road does not satisfactorily explain overshoots in friction force responses that are noticed in field tests, during sudden braking [2].

On the other hand, research results of friction effects in various mechanical systems during the last 30 years point out that the static friction model cannot satisfactorily describe friction force behavior in cases when abrupt change in sliding speed exists. Instead, the dynamic friction models need to be used [3] to [10]. Friction force between the sliding layer of the car tire and the road has a strong dynamic characteristic, i.e. at transition from the adhesion region to the sliding region, an exceptionally fast change in sliding speed occurs from approximately zero speed to the value that corresponds to the sum of the car speed and the sliding speed. Hence, it is justifiable to assume that a static model will not satisfactorily describe friction force behavior.

With the purpose to better understand the dynamic behavior of friction force in contact patch between the car tire and the road, an appropriate laboratory model for experimental research has been designed. It is described in section 2 (more detailed description is given in [11] and [12]) and some experimental results are given in section 3. These results clearly confirm that a dynamic friction model has to be used in order to describe friction force in contact between the car tire and the road. Moreover, the results

---

*Corr. Author's Address: Volumtran, 6 rue Georges Forest, 60200 Compiegne, France, a.bozic@volumtran.com

indicate that both, the brush friction model [8] and [11] and the LuGre friction model [6] to [8], [10], [13] and [14] (both described in section 1), which are most commonly used dynamic models, might be physically incorrect regarding the change of friction coefficient for an asperity bristle passing through the contact surface. In order to model this phenomenon we propose a modification of the LuGre friction model in section 4. Section 5 consists of concluding remarks.

1 DYNAMIC FRICTION MODELING

Static friction models describe dependency of the friction force between two sliding surfaces and their relative speed, i.e. sliding speed. However, apart from the sliding speed, friction force depends dynamically on many other parameters, therefore, dynamic friction models should be used instead of static ones. According to [1] the processes in the place of contact between the car tire and the road can be satisfactorily described with a dynamic tire model. The form of stress distribution in the place of contact used in this model is determined by the kinematics of rolling external strip of the tire. The contact between the tire and the road is realized by the contact surface (patch) of specific length. Contact surface itself is represented by a string of elastic asperity bristles without mass and attenuation (Fig. 1).
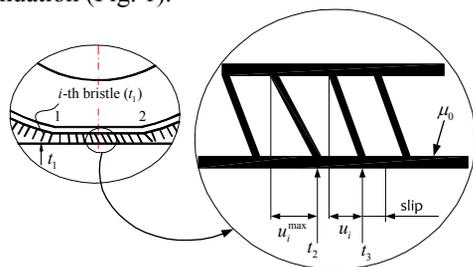
Fig. 1. *Propagation of asperity bristle deformation in contact patch between the car tire and the road*

According to Fig. 1, the contact between the tire and the road begins in point 1 and ends in point 2. After establishing the contact between the top of asperity bristle and the road (time instant t_1) deformation of bristle takes place, i.e. the force in contact point of its top and the road gradually

grows. However, the top of bristle itself is still relative to the road and the relative speed between the top of bristle and the road equals zero. When the bristle reaches maximal deformation u_i^{max} (time instant t_2), relative speed between the top of the bristle and the road abruptly grows (time instant t_3).

According to Fig. 2 where deformations of asperity bristles passing over the contact patch are presented, kinematics of i-th bristle deformation can be described with the following expression [1]:

$$du_i = \frac{\delta u_i}{\delta t} dt + \frac{\delta u_i}{\delta s} ds, \quad i = 1,...,n. \qquad (1)$$

where s is the bristle position on the contact patch relative to the entering point and n is the number of the bristles. At the entering point of contact patch there is no deformation of the bristle, i.e.

$$\frac{du_1}{dt} = 0. \qquad (2)$$

Expression (1) consists of two terms. The first term describes temporal variation of single bristle deformation caused by relative speed v_r. The second term called the convectional term describes the propagation of deformation variation across the contact surface.

If the deformation of the single bristle is observed from the coordinate system tied to its root, which is analogical to the situation when the tire is still and the base moves, convectional part of expression (1) equals zero and expression (1) becomes:

$$du_i = \frac{\delta u_i}{\delta t} dt . \qquad (3)$$

This form is favorable for the description of friction dynamics on the laboratory model because the laboratory model has a moving base, while tire elements are still.

The most often used dynamic friction models are the *reset-integrator (brush) model* and the *LuGre model*, and dynamic friction models of the car tire found in literature are based on one of these models.

1.1 Reset-integrator (brush) Friction Model of the Car Tire

Temporal variation of a bristle deformation is described with expression [1]:
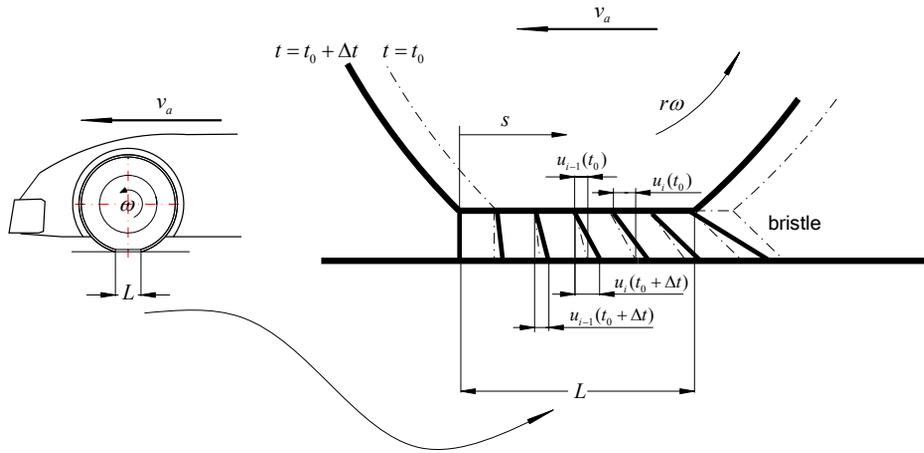
Fig. 2. *Kinematics of asperity bristles deformation passing over the contact patch*

$$\frac{du_i}{dt} = \begin{cases} v_a - r\omega, & c_i u_i < F_{Ni}\mu_s, \\ 0, & c_i u_i = F_{Ni}\mu_c, \end{cases} \quad (4)$$

where v_a is car speed, ω is wheel rotational speed, r is wheel radius, c_i is bristle rigidity constant, F_{Ni} is the local vertical force that depends on the vertical strain distribution in contact patch, μ_s is the adhesion friction coefficient, μ_c is the sliding friction coefficient obtained from any static friction model that gives unique dependency between the friction coefficient and sliding speed [8] and [11]. From (4) it can be seen that the brush model is very simple. If momentary force in the bristle ($c_i u_i$) is lower than the momentary available friction force ($F_{Ni}\mu_s$), the top of the bristle is in contact with the base and the value of bristle deformation grows with the sliding speed (v_a-$r\omega$). When the force in the bristle reaches the value of momentary available friction force, sliding of the top of bristle occurs and bristle deformation stops increasing. Thus, in sliding regime the value of bristle deformation is determined with the momentary available friction force, which is equal to the product of the normal force and sliding friction coefficient. The procedure for determining the parameters of this model is given in [10].

By combining Equations (4) and (1) it is obtained:

$$du_i = (v_a - r\omega)dt + \frac{\delta u_i}{\delta s}ds, \quad i = 1,...,n. \quad (5)$$

As it is (Fig. 2):

$$ds = r\omega dt , \quad (6)$$

Eq. (5) can be written as (this is the final expression of brush model) [11]:

$$\frac{du_i}{dt} = v_a - r\omega - \frac{\delta u_i}{\delta s}r\omega, \quad i = 1,...,n. \quad (7)$$

In computer implementation of this model, partial derivatives $\frac{\delta u_i}{\delta s}$ is approximated with backward difference, which gives $(u_i - u_{i-1})/\Delta s$, with integration step [11]:

$$\Delta t < \frac{\Delta s}{r\omega} \quad (8)$$

As seen from Eq. (4), according to this model the value of the friction coefficient momentarily changes from the value that corresponds to the adhesion friction coefficient to the value that corresponds to the sliding friction coefficient. The distribution of deformation of the string of bristles along the contact surface can be observed through the positional dependency of a single bristle deformation [15], if time is expressed via the known path and speed values:

$$dt = \frac{ds}{r\omega} . \quad (9)$$

For reasons of simplicity, uniform distribution is considered. According to Eq. (4) the maximal deformation is:

$$(5) \quad u_i^{max} = \frac{F_{Ni}\mu_s}{c_i} . \quad (10)$$

$$ds = r\omega dt , \quad (6)$$

(6)

From Eqs. (9) and (4) the rate of deformation growth in dependency of crossed path is obtained:

$$\frac{du}{ds} = \frac{v_a}{r\omega} - 1. \tag{11}$$

According to Eq. (2) the initial bristle deformation equals zero, and thereafter its deformation grows linearly with the slope given by Eq. (11) until the maximal deformation, given by Eq. (10), is reached. A schematic description of a bristle deformation in dependency of crossed distance on the path through the contact surface is given in Fig. 3. The solid line represents the deformation of the bristle in dependency of its position on the path through the contact surface. A step change of deformation from the value corresponding to the adhesion friction coefficient to the value corresponding to the sliding friction coefficient is noticeable. This discontinuity is not physical [8]. A dashed line represents gradual change, which more closely resembles reality. Additional simplification in the brush friction model pertains to neglecting the dumping in the sliding layer bristles.

To avoid difficulties in mathematical modeling and analysis of friction influence that are caused by discontinuity in model (4), other friction models are developed. One of the best-known models is the so called LuGre friction model [6] and [7].
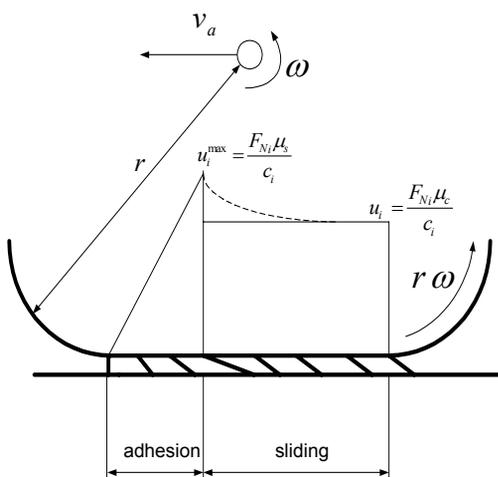
Fig. 3. *Propagation of a bristle deformation on its path through the contact surface for brush tire model*

1.2 LuGre Friction Model of the Car Tire

The LuGre friction model describes the change of friction force through the change of deformation of asperity bristles [6], [7], [8] and [10]. Asperity bristles are microscopic thin bristles ($\approx 5 \cdot 10^{-6}$ m) through which contact between two bodies is established (Fig. 4).
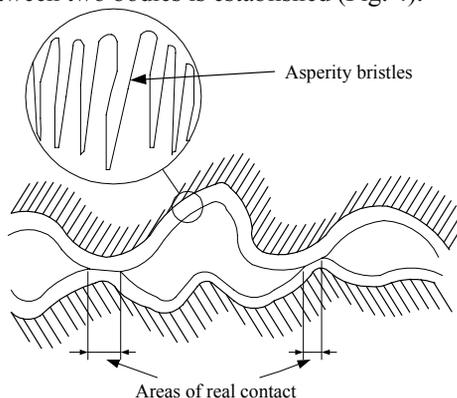
Fig. 4. *Contact of two bodies through asperity bristles*

The change of asperity bristles deformation z is described with expression:

$$\frac{dz}{dt} = v - \frac{\sigma_0}{F_N g(v)} z |v|, \tag{12}$$

where z is the deformation of the asperity bristles, v is the relative speed between the tops of asperity bristles of contact bodies, σ_0 is the rigidity constant of the bristles, v_0 is the Stribeck speed, F_N is the normal force, $g(v)$ is the function that describes dependency of bristles deformation on relative speed.

Function $g(v)$ in the LuGre friction model is given by:

$$g(v) = \theta(a_o + a_1 e^{-(v/v_0)^{0.5}}). \tag{13}$$

where v_0 is the Stribeck speed.

In Eq. (13) the sum ($a_0 + a_1$) corresponds to the static friction coefficient, a_0 corresponds to the Coulomb friction coefficient, θ is a correction coefficient that depends on the base type. The total friction force is calculated as:

$$F_f = \sigma_0 z + \sigma_1 \frac{dz}{dt} + F_N a_2 v, \tag{14}$$

where a_2 is the viscosity friction coefficient. The procedure for determining the parameters of LuGre model is given in [10].

The dynamic friction model of the car tire based on the LuGre friction model is proposed in [13], [14] and [17]. The dynamics of the bristles deformation of the sliding pair rubber/asphalt is approximated with the dynamics of microscopic asperity bristles. By inserting Eq. (12) in Eq. (1), and putting $u_i = z$ i $v = v_r = v_a - r\omega$, the following partial differential equation is obtained:

$$\frac{du_i}{dt} = v_r - \frac{\sigma_0 u_i}{g(v_r)}|v_r| - \frac{\delta u_i}{\delta s} r\omega, \ i = 1,...,n \ , \quad (15)$$

where:

$$g(v_r) = \theta(a_o + a_1 e^{-(v_r/v_0)0.5}) \ . \quad (16)$$

Equations (15) and (16) describe the LuGre friction model in the contact patch between the car tire and the road. In computer implementation of this model it is necessary to approximate the partial derivatives $\frac{\delta u_i}{\delta s}$ with backward differences $(u_i - u_{i-1})/\Delta s$.

2 LABORATORY MODEL CONSTRUCTION

A laboratory model is designed in order to get an insight into dynamic behavior of the friction force in contact patch between the car tire and the road by means of an experiment. More specifically, the goal of the laboratory model design is to test if the friction coefficient for an asperity bristle changes during its passing through the contact surface. If it changes, then none of the existing dynamic friction models (described in previous section) satisfactorily describe the tire-asphalt sliding pair dynamics and a new friction model should be developed.

As explained in the previous section, the mathematical model of the tire consists of two terms: (i) the term relating to temporal variations of a single bristle deformation caused by relative speed v_r and (ii) the term relating to the rotation of the tire. Since only the first term is of interest for our research, there is no need to implement the tire rotation on the laboratory model. Therefore, for experimental verification, the laboratory model only needs a small part of a tire (e.g. a tire element of size approx. 1 x 1cm), which represents a bristle going through the contact patch. That tire element can be static and fixed to the measuring equipment, which is able to record normal and friction forces acting on it.

The support of the measuring equipment has to allow variation of the normal force in order to verify its influence on the variation of the friction force, and consequently on variation of the friction coefficient. The movable part of the laboratory model has to simulate only relative speed between the tire element and the road ($v_r = v_a - r\omega$).

Since the tire element represents a small element of the sliding layer of the car tire, it can be implied that similar conditions exist over the entire surface, i.e. the same amount of normal pressure forces and sliding speeds. Such a tire element corresponds to a bristle in dynamic brush model [15]. As seen from Fig. 5, the tire element on tire circumference is highly dynamically stressed. Before a tire element comes into contact with the road, there is almost no force acting on it. Just after the tire element comes into contact with the road, normal pressure acting on it increases rapidly. The difference between the wheel circumferential speed and car speed during braking causes the deformation of the tire element. During this deformation there is practically no sliding between the road and the tire elements, i.e. the tire element is in adhesion region. When stresses in the tire element caused by its deformation, cross their limit value, which is determined by the product of maximum value of friction coefficient μ_{max} and the value of normal force F_N, further deformation of the tire element is not possible and sliding occurs. On real cars, the tire would start rotating at that moment and the tire element would experience reduction of the deformation due to the reduction of the normal force toward the end of the contact patch. But as already mentioned, this effect is not of interest for our research. The region that is at the focus of our experimental verification is annotated in Fig. 5. It ranges from time instant when the contact between the tire element and the road is established to time instant when the deformation is stabilized i.e. when the tire element starts to slide over the road.

As the base for constructing the laboratory model for experimental research of dynamic processes in the contact patch between rubber and asphalt, an existing laboratory model for research of friction, elasticity and backlash effects is used. This model is located at the Faculty of Electrical Engineering and Computing, University of Zagreb.
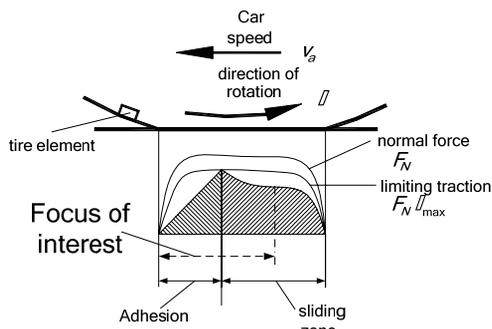
Fig. 5. *Stress of a tire tire element during its passing over the contact patch in case of breaking*

2.1 Original Laboratory Model

The photograph and the scheme of the original laboratory experimental model are shown in Figs. 6 and 7, respectively [11] and [12]. As seen from the figures, the laboratory model has the cylinder chassis (4) as its base. It consists of two servo units (3) with embedded resolvers (2) for magnetic field control of the motors and incremental encoders (1) with a resolution of 120000 pulses/revolution for very accurate measurement of the speed and the position of servo drives. Since both motors have equal characteristics, each of them can be used either as a driving motor or as a load motor without any significant modification. On both sides of the laboratory model there are changeable inertial discs (5). By changing the number of discs on one or both sides of the laboratory model it is possible to change the inertial ratio between the sides. The

sides of the laboratory model can be connected via a changeable shaft (6), which can be of different diameters. This connection can be made with or without a backlash. The backlash is realized by a specially designed connection subsystem (7) of the changeable shaft (6) to the main shaft (9).

2.2 Modified Laboratory Model

In order to enable experimental investigations of the described physical processes in the contact patch of the car tire and the road, the laboratory model should enable execution of the following functions:
- generation of the variable pressure force;
- generation of the friction force;
- generation of the variable sliding speed;
- measuring of the normal pressure force and the friction force;
- measuring of the sliding speed.

Since generation of the friction force as well as generation and measurement of the variable sliding speed have already been solved on the original laboratory model, the modifications of it should enable execution of the remaining functions. Fig. 8 shows the general scheme of the laboratory model with the modified structure of the electromechanical system, which is adapted for testing of the dynamic behavior of the rubber-asphalt sliding pair. A more detailed description of the laboratory model is given bellow in subsections 2.2.1 to 2.2.4.

Fig. 6 *Original laboratory model*

1. Incremental encoder
2. Resolver
3. Servomotor
4. Chasis
5. Additional inertia discs
6. Changeable shaft
7. Backlash generating subsystem
8. Holder of the shaft bearing
9. Main shaft
10. Fastening ring
11. Braking disc
12. Fastening plate
13. Fastening screws
14. Holding foil springs
15. Holder of braking subsystem
16. Measuring body with the strain gauges
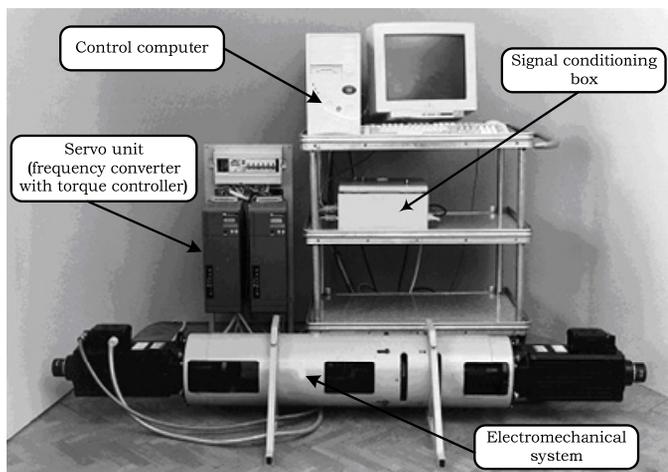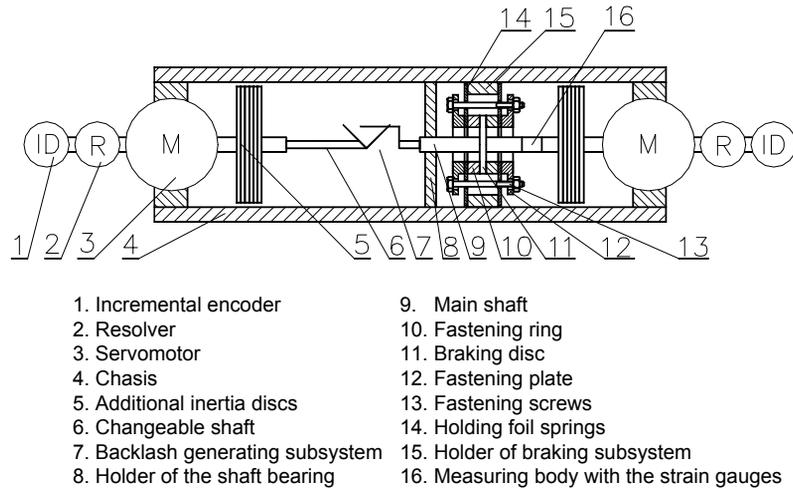
Fig. 7 *Scheme of the original laboratory electromechanical system*

1. Incremental encoder
2. Resolver
3. Servomotor
4. Chasis
5. Additional inertia discs
6. Changeable shaft
7. Rotation-to-translation converter
8. Holder of the shaft bearing
9. Main shaft
10. Subsystem for friction torque measurement
11. Asphalt holder
12. Subsystem for pressure force measurement
13. Self-adjusting bearings
14. Holding foil springs
15. Holder of the measuring system

Fig. 8. *General scheme of the structure of the modified electromechanical system*

Comparing the scheme in Fig. 8 to the scheme in Fig. 6 it is easy to notice the modifications of the original laboratory model. The subsystem for backlash generation ((7) in Fig. 6) is replaced with a subsystem that converts rotation into translation ((7) in Fig. 8). This subsystem converts the torque of the driving motor into the force that determines the pressure in the sliding pair. By changing this torque it is possible to change the pressure in the sliding pair during the experiment. The pressure ring ((10) in Fig. 6) is replaced with a subsystem for friction force measurement ((10) in Fig. 8). The asphalt holder (11) is added to the braking disc. The subsystem for torque measurement is connected to the subsystem for pressure force measurement (12) through the self-adjusting ball bearings (12). The subsystem for pressure force measurement is also connected through the self-adjusting ball bearings to the bearing plates (14), which are held by the measuring device holder (15) that fixes the whole system to the chassis of the laboratory model. Thus, four additional subsystems are developed: a) the subsystem for friction generation, b) the subsystem for friction torque measurement, c) the subsystem for pressure force measurement and d) the subsystem for pressure force generation. These subsystems are described in succession.

2.2.1 Subsystem for Friction Generation

The subsystem for friction generation consists of two main parts: the asphalt holder and the rubber holder. The asphalt holder is movable and is mounted on the shaft of the laboratory model, while the rubber holder is still and mounted on a fixed measuring device. The scheme and the photograph of the asphalt holder are shown in Figs. 9 and 10, respectively. The rubbing ring (4) is fixed to the shaft of the laboratory model (1) with a pressing plate (2) and screws (3). The asphalt (5) is inserted into a groove on the asphalt holder. In order to prevent the asphalt from slipping out of the groove, the maximal diameter of the groove is smaller than the maximal diameter of the asphalt. The outer lining of the groove prevents the asphalt from cracking or slipping out under the influence of centrifugal force. The rubber holder is integrated into the subsystem for friction torque measurement and is described together with it.

2.2.2 Subsystem for Friction Torque Measurement

Friction is measured using the strain gauges glued onto appropriate segments of the construction. The scheme of the subsystem for friction measuring is given in Fig. 11a, and looks a lot like the system for torque measurement on the robot PUMA 500 [16]. The subsystem consists of two rings interconnected with four rectangle holders. The front ring is also the holder for the tire elements. There are 3 tire elements, equally spaced, in order to provide zero friction force components in y and z directions (Fig. 12),
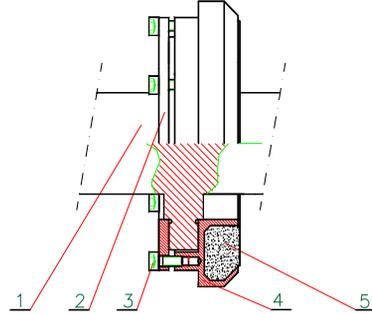
Fig. 9. *Asphalt holder: shaft (1), pressing plate (2), fastening screw (3), rubbing ring (4), asphalt (5)*

Fig.10. *Photograph of asphalt holder: shaft (1), pressing plate (2), fastening screw (3), rubbing ring (4), asphalt (5)*
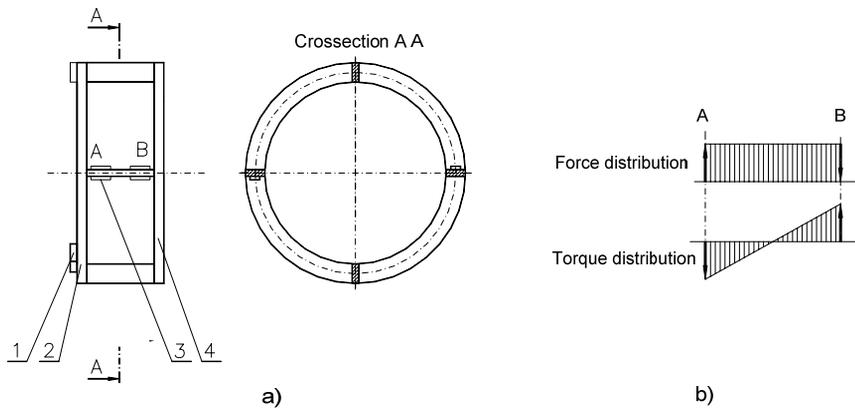
Fig. 11. *Subsystem for friction torque measurement: a) scheme of the subsystem for torque measurement: tire element (1), front ring (2), holder with strain gauges (3), rear ring (4); b) stress on one of the holders caused by friction*

accordingly pure torque action around x axis will be generated. The rear ring serves as a junction with the rest of the construction (not shown in the figure). The friction force on tire elements is transferred to the front ring which causes it to turn and that brings about the deformation of the holders. The four strain gauges glued on the holder segments with the maximal stresses are connected in a full Wheatstone bridge giving voltage signal proportional to the holders' deformations, i.e. the friction force. Maximal stresses occur on the edges of the holders, as shown in Fig. 11b. The tire elements are obtained by cutting rectangular pieces from a real car tire, and are fixed on the front ring with mechanical fasteners.

2.2.3 Subsystem for Pressure Force Measurement

The scheme of the subsystem for pressure force measurement is shown in Fig. 12. It has the form of a frame that connects the subsystem for friction torque measurement and the holder of the measuring system, i.e. the chassis of the laboratory model. Two pairs of self-adjusting bearings are placed in this frame. The first pair forms a rotation axis around the *y*-axis of the coordinate system related to the frame. The subsystem for pressure force measurement rotates around this axis. The other pair of bearings forms a rotation axis around the *z*-axis of the coordinate system related to the holder of the measuring system. The frame, together with the subsystem for friction torque measurement, rotates around this axis. In this way the subsystem for friction

torque measurement, together with the tire elements, has two degrees of freedom. This insures a good contact between the tire elements and asphalt. The strain gauges for pressure force measurement are glued on segments of the frame with decreased cross-sections. Since the frame was mounted using self-adjusting bearings, deformation of segments on which the strain gauges are glued can be regarded as pure bending, as shown in Fig. 12. The photograph of the measuring system is given in Fig. 13, where the subsystem for pressure force measurement can be clearly seen.

2.2.4 Subsystem for Pressure Force Generation

This is a lever mechanism that converts rotation into translation, i.e. it converts the motor torque into pressure force. The scheme and the photograph of this subsystem are shown in Figs. 14 and 15, respectively. The suspender of the measuring system can be seen as a part of the fastening subsystem because it behaves like a spring and moves the tire elements away from the asphalt. The suspender itself consists of foil springs. The location of foil springs provides a fairly simple axial shift of the tire elements, generating the pressure force on the sliding pair. At the same time the spring system must provide a rigid transfer of the torque generated by friction to the chassis of the laboratory model (without a backlash and with negligible bending). By proper dimensioning of the foil springs it is possible to adjust the stiffness of the spring system.
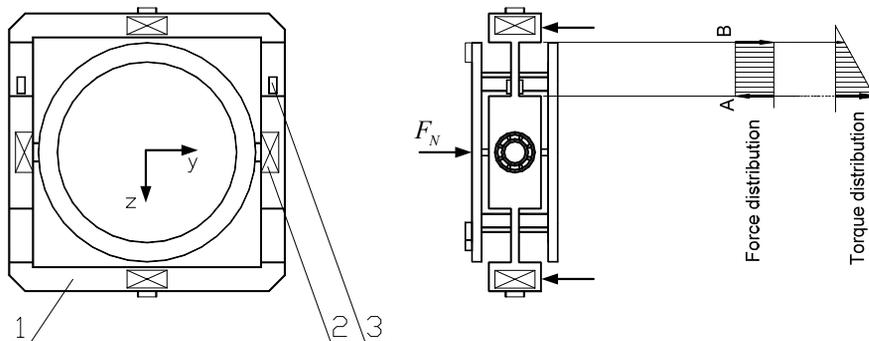
Fig. 12. *Subsystem for pressure force measurement with the stress diagram on the measuring segment: frame of the subsystem (1), self-adjusting ball bearing (2), strain gauges (3).*
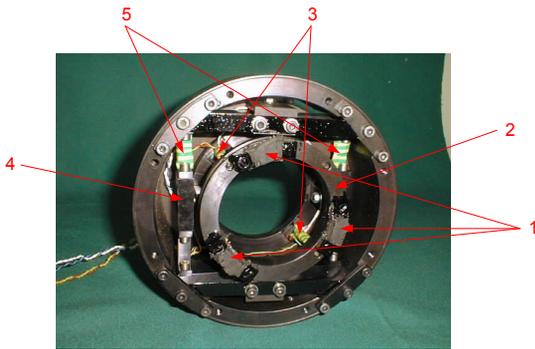
Fig. 13. *Photograph of the measuring system: tire elements (1), subsystem for friction torque measurement (2), strain gauges of the subsystem for friction torque measurement (3), subsystem for pressure force measurement (4), strain gauges of the subsystem for pressure force measurement (5)*

crossection A — A

$$F_m = \frac{m}{l_1} \qquad F_n F_m = \frac{l_2}{l_3}$$

Fig. 14. *Subsystem for pressure force generation: shaft of the subsystem (1), adjusting shell (2), constant arm lever (3), variable arm lever (4), clue (5), fastening screw (6)*

Figs. 16a and b show two variants of the foil spring: foil strip and foil plate, respectively. Foil strips are less stiff, but very sensitive to the overload of the spring system. The mechanism of the subsystem for generating the pressure force must overpower the spring force. This means that springs with smaller stiffness will give greater pressure force. In the laboratory model, a combination of both variants of foil springs is used as a compromise between stiffness and robustness. Foil strips are positioned on the front side and a string plate on the rear side (Fig. 17).

Fig. 15. *Photograph of the subsystem for pressure force generation*

foil strip

foil plate

a) b)
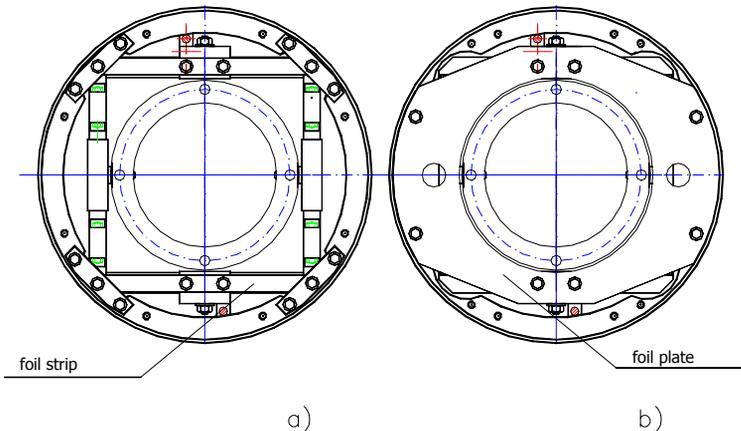
Fig. 16. *Two variants of the spring carrier: a) foil strip, b) foil plate*

3 EXPERIMENTAL RESULTS

As already mentioned, the described laboratory model was assembled in order to conduct investigate the dynamical characteristics of the friction force in the contact patch between the car tire and the road by means of an experiment. In this section the results of the experiment are presented. They confirm the functionality of the laboratory model and provide possible shortcomings of the existing dynamic friction models in modeling the friction force between a tire element and asphalt.

When conducting experiments on the laboratory model, the pressure force (corresponds to the normal force in the car) is generated by an adequate torque reference value given to the left motor in Fig. 8 (hereafter labeled as motor M1). The generated torque converts the pressure force via the mechanism of pressure force generation (Figs. 14 and 15). The desired sliding speed is generated through the regulation of angular speed of the right motor in Fig. 8 (hereafter labeled as motor M2), and consequently the regulation of angular speed of asphalt holder that is fixed to the motor axis.

Fig. 17. *Photograph of the measuring system*

In order to test if the overshoot in friction force exists at transition from the adhesion zone to the sliding zone, four experiments were conducted, results of which are shown in Figs. 18 to 21. The focus of interest is marked on graphs in all figures.

All four experiments were conducted in the same manner, differing only in the sliding speeds. At the beginning of each experiment the pressure force was generated using 5.5% of the rated torque of the motor M1. Thereafter, at time instant $t = 3.5$ s a step change of the angular speed of the motor M2, and consequently of the sliding speed, was done: from 0 rpm to 10 rpm in the first experiment (Fig. 18), from 0 to 20 rpm in the second experiment (Fig. 19), from 0 to 30 rpm in the third experiment (Fig. 20) and from 0 to 120 rpm in the forth experiment (Fig. 21). Then, at time instant $t = 4$ s, in all experiments, a step change of reference torque of the motor M1 was given from 5.5 to 40% of the rated torque, which caused a sudden change of the friction force (torque). The low-pressure force at the beginning of all the experiments provided good coherence between the tire elements and the asphalt base during acceleration in time interval from $t = 3.5$ s to $t = 4$ s. Sliding in time interval from $t = 3.5$ s to $t = 4$ s, with low-pressure force matches the situation when a sliding layer element of the car tire enters the contact with asphalt (Fig. 3). The upswing of the pressure force matches the situation of the tire element passing trough the adhesion zone. Dumped oscillations in settling of the pressure force that occur in laboratory model do not exist in real tires. At lower sliding speeds (10, 20 and even 30 rpm), an overshoot in friction force occurs after the transition process of the pressure force ends (Figs. 18 to 20). Therefore, the influence of oscillations in the settling of pressure force can be neglected at lower sliding speeds. The overshoot in friction force (torque) is clearly visible even at a sliding speed of 120 rpm (Fig. 21). In this case, an overshoot in friction torque (force) coincides with the overshoot in pressure force. However, when the pressure force later takes the value equal to the one it had during the first overshoot, the friction torque (force) remains at a steady state value, which is significantly lower than the value it had during the first overshoot. This suggests that the first overshoot in friction force is not solely a consequence of the overshoot in pressure force, but also of the dynamic behavior of friction itself.

In order to investigate the damping inside the tire element, two additional experiments were undertaken. Both experiments were conducted with motors in standstill, so that the influence of friction on the inner tire element damping could be ignored. This was achieved by applying the small values of motor torques. In the first additional experiment the pressure force was

generated by applying the reference torque to motor M1 of 60% of its rated torque value, while the motor M2 was working without the speed regulation and with sinus reference torque of 2 rad/s frequency and of 30% rated motor torque amplitude. The result of this experiment is shown in Fig. 22 where x-axis represents turn angle of the motor M2 and y-axis represents its torque, which corresponds to the force in the tire element. Hysteresis dependence of the force in the tire element on the change of the turn angle indicates loss existence due damping in the tire element.
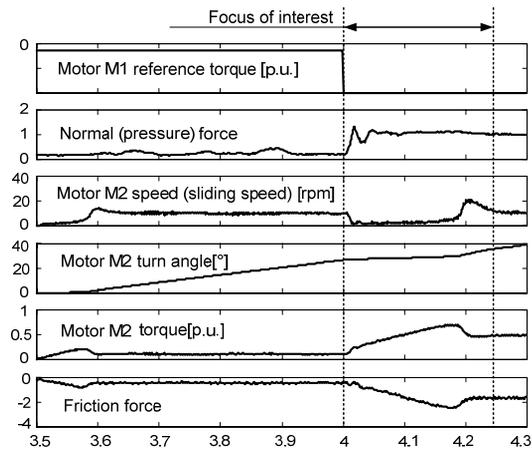
Fig. 18. *Responses obtained at sliding speed of 10 rpm*
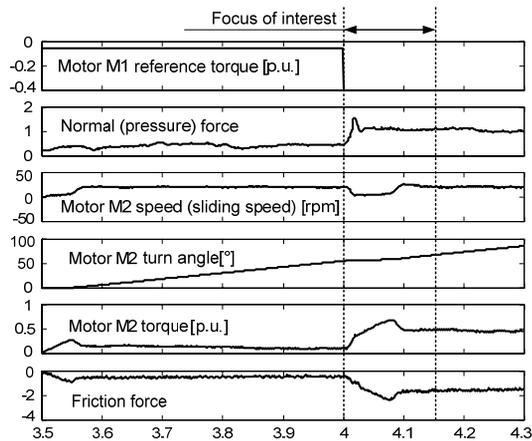
Fig. 19. *Responses obtained at sliding speed of 20 rpm*

In the second additional experiment the pressure force was again generated by applying the reference torque to motor M1 of 60% of the rated torque value. But, in this experiment the sliding pair rubber/asphalt was exposed to a step

change of reference torque of motor M2 of 60% of the rated torque value. The response of the actual torque of motor M2 is shown in Fig. 23. A strong damping can be noticed in the response.
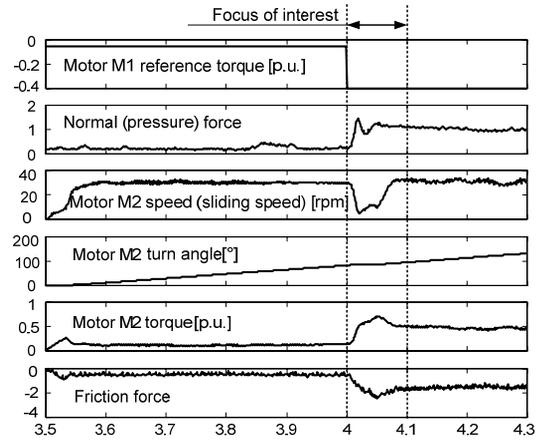
Fig. 20. *Responses obtained at sliding speed of 30 rpm*
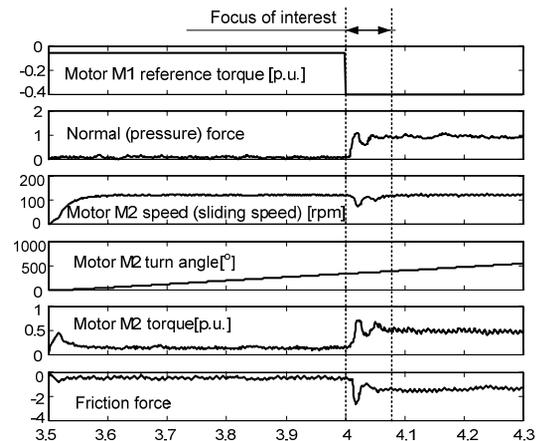
Fig. 21. *Responses obtained at sliding speed of 120 rpm*

On the basis of overshoots in friction force and damping inside the tire elements that are experimentally confirmed, a tire element deformation dependent on the crossed path during its passing through the contact surface is qualitatively drawn in Fig. 24 (dashed line). Fig. 24 also shows the tire element deformation for the brush friction model of the car tire [8] and [11] (solid line) and for LuGre friction model of the car tire [13] and [17] (dotted line).

While the LuGre model of the tire cannot describe the overshoot at all, the brush model of the tire describes the overshoot but with a non-physical discontinuity, which occurs because the

Božić, A. - Petrović, I. - Matuško, J.

brash model neglects damping inside the tire elements.
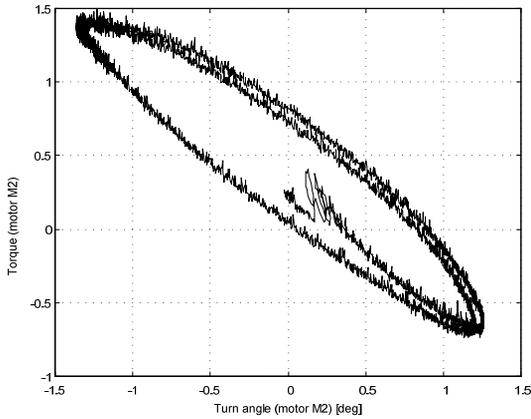
Fig. 22. *Tire element hysteresis*
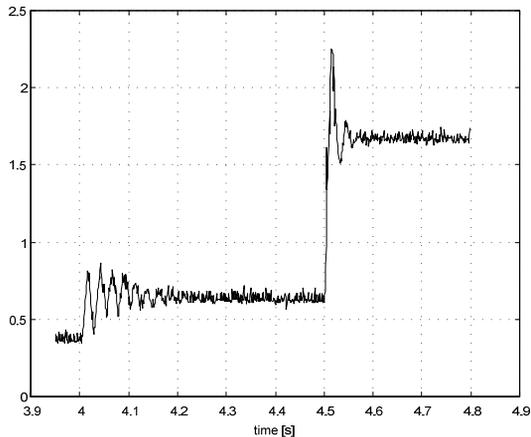
Fig. 23. *Response of the torque of motor M2 to the step change of its reference value*

4 PROPOSITION FOR MODIFICATION OF THE LUGRE FRICTION MODEL OF THE CAR TIRE

The LuGre friction model given by Eqs. (15) and (16) proved adequate in modeling the static friction characteristics of the car tire [13], but its ability for modeling the dynamical friction characteristics has not yet been confirmed. A possible drawback of this model is that it describes changes of friction force over deformations of the asperity bristles, which are in range of $5 \cdot 10^{-6}$ m, whereas during laboratory model assembly and testing it was found that the deformation of the tire elements of the sliding layer was grater than 1mm.
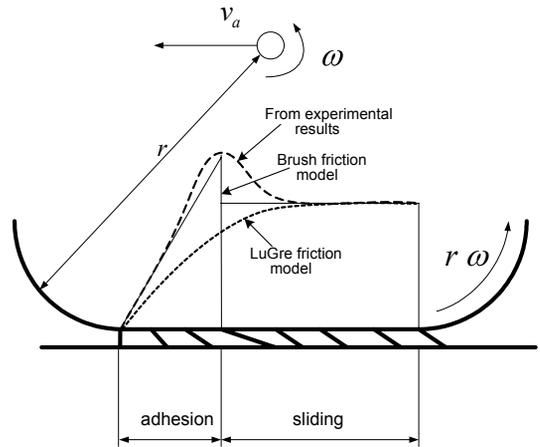
Fig. 24. *Propagation of tire element deformation on its path through the contact surface.*

The deformation of a single tire element of the sliding layer is shown on Fig. 25, where it can be seen that a rubber element consists of the string of asperity bristles and that all of them have equal sliding speed given by:

$$v = v_r - \frac{du_i}{dt}. \tag{17}$$

By inserting Eqs. (17) in (13) the function $g(.)$ for i-th tire element becomes:

$$g_i(v_r - \frac{du_i}{dt}) = \theta(a_o + a_1 e^{-((v_r - \frac{du_i}{dt})/v_0)0.5}), \tag{18}$$

$$i = 1, \ldots, n$$

from which and from Eq. (15) the following partial differential equation of car tire friction model is obtained:

$$\frac{du_i}{dt} = v_r - \frac{\sigma_0 u_i}{g_i(v_r - \frac{du_i}{dt})}|v_r| - \frac{\delta u_i}{\delta s} r\omega, \tag{19}$$

$$i = 1, \ldots, n.$$

Thus, the proposed friction model differs from the original LuGre model in the way function $g(.)$ is calculated. While in the original LuGre model function $g(.)$ is of constant value for the entire contact surface, in the proposed model it takes different values for each of n tire elements. Fig. 26 shows the tire element deformation in the dependency of crossed path during its passing through the contact surface for both models.
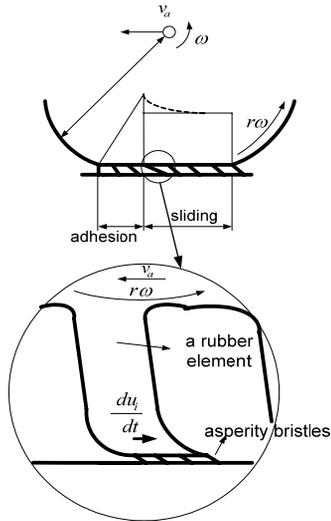
Fig. 25. *Interaction between tire elements and asperity bristles of the sliding layer*

Fig. 26. *Propagation of tire element deformation on its path through the contact surface for the original LuGre model (solid line) and for the proposed modified LuGre model (dashed line)*

While the tire element deformation calculated according to Eqs. (18) and (19) is plotted with a dashed line, the tire element deformation calculated according to equations (15) and (16) is plotted with a solid. It can be noticed that the proposed model gives an overshoot at the transition from the adhesion zone to the sliding zone. Namely, from the relations (4), (12) and (17) it follows that in the adhesion zone sliding speed of the asperity bristles of a tire element equals zero ($v = 0$), so that function $g(.)$, calculated according to Eq. (18), takes its maximal value, and consecutively, so does the friction coefficient. When the force in the tire element takes its maximal value, which corresponds to the maximal value of the friction coefficient, sliding occurs. In sliding regime, according to (4), du_i/dt falls to zero, thereof the friction coefficient and consequently the friction force take values that are related to the difference between the car speed and the tire circumferential speed (v_a-$r\omega$). This change in the sliding speed induces an overshoot in the friction force [6], [7] and [10], as it is shown in Fig. 26. The original LuGre friction model does not give an overshoot, because the function $g(.)$, calculated according to (16), takes a constant value over the entire contact surface, and consequently the friction coefficient has a constant value too.

As stated in [2] and [17], the friction coefficient changes its value at transition from the adhesion zone to the sliding zone. Hence, it is justifiable to suppose that the friction model with $g(.)$ calculated according to Eq. (16) cannot correctly describe the dynamics of the car tire friction force. A proposed friction model with $g(.)$ calculated according to Eq. (18) offers an appropriate solution for this problem.

The above described shortcoming of the original LuGre friction model is additionally proved by experimental results in [2], where it is shown that the static characteristic of the friction coefficient (curve g_{EX} in Fig. 27) has a bell shape with the maximum at a certain sliding speed (v_m), while the LuGre model gives the maximal value of the friction coefficient at zero sliding speed (curve g_{LG} in Fig. 27), which is determined by exponential function (16). From Fig. 27, it can be seen that the LuGre model describes the real tire
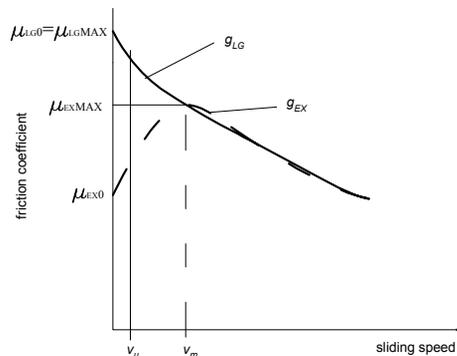
Fig. 27. *Friction coefficient versus sliding speed*

characteristic for the sliding speeds above v_m well, but for sliding speeds below v_m a remarkable depart occurs. In further research and development of the car tire friction models, it is necessary to investigate how much this depart can influence the quality of the friction force estimation, especially when a car is on inclined road and at the boundary value of friction force.

5 CONCLUSIONS

A laboratory model for experimental investigations of dynamic friction force behavior in the contact patch between the car tire and asphalt was designed and built. The results of the conducted experiments on the laboratory model point out the possible difficulties in modeling of dynamic friction characteristics. They indicate that both, the brush tire friction model and the LuGre tire friction model cannot physically correctly describe the dynamics of friction in the contact patch between the car tire and road. However, for a final confirmation of the arguments presented in this paper we propose field tests on real cars. These tests should include the recording of the dynamical friction force behavior after the pounce of the car breaking torque as well as during its slow-ramp increase. As the active vehicle dynamic control systems correct the car trajectory by generating short-term step changes of the breaking/accelerating torque, the experiments should embrace the results obtained with different values of friction torque steps, particularly in the area of maximal friction force values. The results of these field tests should be compared to the simulation results based on the existing friction models. If a difference is observed like in our experiments, then the existing friction models should be modified in order to improve accuracy of the simulations.

6 REFERENCES

[1] Fodor, M., Yester, J., Hrovat, D. (1998) Active control of vehicle dynamics. *In Proceedings of the 17th IEEE/AIAA Digital Avionics Systems Conference (DASC'98), Bellevue, WA*, Oct. 31-Nov. 6 1998.

[2] Clark, S.K. - ed. (1981) Mechanic of Pneumatic Tires, *US Department of Transportation*, NHTSA.

[3] Dahl, P. R. (1968) A solid friction model. Aerospace Report TOR-0158(3107-18)-1, *The Aerospace Corporation*, El Segundo, CA.

[4] Dahl, P.R. (1976) Solid friction damping of mechanical vibrations. *AIAA Journal*, 14(12), p. 1675-1682.

[5] Dahl, P.R. (1977) Measurement of solid friction parameters of ball bearings. *In Proc. of 6th Annual Symp. on Incremental Motion, Control Systems and Devices*, p. 49-60, University of Illinois, ILO.

[6] Canudas de Wit, C., Olsson, H., Aström, K. J., Lischinsky, P. (1995) A new model for control of systems with friction. *IEEE Transaction on Automatic Control*, 40(3), p. 419-425.

[7] Canudas de Wit, C., Lischinsky, P. (1997) Adaptive friction compensation with partially known dynamic friction model. *International Journal of Adaptive Control and Signal Processing*, 11, p. 65-80.

[8] Armstrong-Hélouvry, B. (1991) Control of Machines with Friction. *Kluwer Academic Publishers*.

[9] Haessig, D.A., Friedland, B. (1991) On the modeling and simulation of friction. *ASME Journal of Dynamical Systems, Measurement, and Control*, 113, 354-362.

[10] Božić, A. (2000) Design and identification of electromechanical set-up of servodrive with adjustable torsion, friction and backlash effects. *Master's thesis, Faculty of Electrical Engineering and Computing, University of Zagreb*(in Croatinan).

[11] Božić, A., Petrović, I., Matuško J. (2001) Design and functionality verification of the experimental setup for investigation of the dynamic behavior of the rubber/asphalt sliding pair. *Internal memorandum, University of Zagreb*.

[12] Božić, A. (2001) Experimental setup for investigation of the dynamic behavior of the rubber/asphalt sliding pair. *Project documentation* (In Croatian), *University of Zagreb*.

[13] Canudas de Wit, C., Tsiotras, P. (1999) Dynamic tire friction models for vehicle traction control. *In Proc. of the 38th IEEE*

Conference on Decision and Control, pp. 3746-3751, Phoenix, Arizona, USA.

[14] Deur, J., Matuško, J (2001) Parametrization of lugre tire model for different normal forces. *Internal Memorandum, University of Zagreb*, 25 pages.

[15] Van Zanten, A., Ruf, W.D., Lutz, A. (1989) Measurement and simulation of transient tire forces. *SAE paper 890640*.

[16] Pfeffer, E.L., Khatib, O., Hake, J. (1989) Joint torque sensory feedback in the control of puma manipulator. *IEEE Transaction on Robotics and Automation*, 5.

[17] Deur, J., Asgari, J., Hrovat, D. (2001) Modeling and analysis of longitudinal tire dynamics based on the Lugre friction model. *In 3rd IFAC Workshop, Advances in Automotive Control, Vol. 1,* Karlsruhe, Germany.